Towards ultra-high gradient particle acceleration in carbon nanotubes

Journal of Physics: Conference Series **1596** (2020) 012028 doi:10.1088/1742-6596/1596/1/012028

Towards ultra-high gradient particle acceleration in carbon nanotubes

A Perera[1,3], A Bonatto[2,3], C Bonţoiu[1,3], J Resta-López[1,3], V Rodin[1,3], C Welsch[1,3], G Xia[2,3], and G Yadav[1,3]

[1] Department of Physics, University of Liverpool, Oxford Street, Liverpool L69 7ZE, UK
[2] Department of Physics and Astronomy, University of Manchester, Oxford Road, Manchester, M13 9PL, UK
[3] Cockroft Institute, Keckwick Ln, Daresbury, Warrington WA4 4AD, UK

E-mail: aravinda.perera@liverpool.ac.uk

Abstract. Charged particle acceleration using solid-state nanostructures is attracting new attention in recent years as a method of achieving ultra-high acceleration gradients in the order of TV/m. The use of carbon nanotubes (CNTs) has the potential to overcome limitations of using natural crystals, e.g. channelling aperture and thermo-mechanical robustness. In this work, we present preliminary particle-in-cell simulation results of laser and beam interaction with a single CNT, modelled as 20 parallel plates of Carbon ions and electrons. This is the equivalent to a 10-layers tube in 3D. We further discuss simulation of anisotropic particles to model 2D quasi-free electrons in CNT walls. Further research ideas are outlined along with the presentation of a possible proof-of-principle experiment.

1. Introduction

Since it was originally proposed over three decades ago [1, 2], there has been a renewed interest in the development of solid-state based particle accelerators. Several schemes have been considered for such an accelerator, including beam-driven [3] and x-ray-driven [3, 4] variants. In particular, it has recently been proposed that charged particle beams channelled through metallic carbon nanotubes (CNT) may be used to excite a number of propagating modes which could in turn be utilised as wakefields for acceleration of further beams [5]. Such modes range from surface plasmon polaritons [6] to highly non-linear electrostatic oscillations [3] involving the quasi-free valence electron gas of the cylindrical graphene layer that makes up the nanotube walls. As opposed to hollow-channel gaseous plasma based accelerators, the very high density of the electron gas, up to $10^{24}\,\mathrm{cm}^{-3}$ in such solid state media has been predicted to allow ultra-high accelerating gradients of up to 1 TV/m. CNTs are generally multi-walled tubular structures with a typical diameter of 1.35 nm and a C-C bond length of 0.14 nm, sitting between the solid- and plasma-state in terms of achievable charge density. For instance, with an average CNT mass density of $1.6\,\mathrm{g/cm}^3$ the maximum ion density is $\sim 10^{22}\,\mathrm{cm}^{-3}$, namely 2-3 orders of magnitude higher than plasma densities currently available in supersonic gas jets. Single-wall CNTs have thermal conduction coefficients of up to $6\,\mathrm{kW/(m\,K)}$ and can sustain current densities of up to $10^9\,\mathrm{A/cm}^2$ [7]. In addition to their reported tensile strength of $\approx$45 GPa, these features make CNTs a very robust target for interactions with laser and charged-particle beams. It has been shown theoretically [2] that TV/m accelerating gradients are possible in a crystal lattice if it

is radiated by a laser of $10^9\,\mathrm{W/cm^2}$ power density and 5 ps pulse length at Bragg angle, as this stimulates the Bormann anomalous transmission [8]. However, laser beams of such X-ray wavelengths cannot be produced in a controllable manner up to date. In this work we present a proposal for a proof-of-principle experiment to demonstrate channelling acceleration in an array of parallel CNTs and report preliminary particle-in-cell (PIC) simulations of laser and beam interaction with single CNTs. Ongoing work in the testing and implementation of a new model of radially bound CNT wall electrons is discussed.

2. Experimental Proposal

Uncontrolled acceleration of charged particles in CNTs following laser irradiation was already demonstrated [9] but controlled synchronous acceleration has not been achieved yet. Thus, based on the future outcome of the simulations, an experiment is planned in order to complete the proof-of-principle acceleration mechanism. Currently operational beam test facilities in Europe, such as the Versatile Electron Linear Accelerator (VELA) and the Compact Linear Accelerator for Research and Applications (CLARA) [10, 11] at Daresbury in the UK and the CERN Linear Electron Accelerator for Research (CLEAR) [12, 13] at CERN in Switzerland, may offer the necessary beam conditions and infrastructure to carry out an experimental demonstration of this concept. A tentative experimental beamline layout is shown in figure 1, where typical beam diagnostics devices to characterise the beam before and after crossing the CNT sample, and a magnetic chicane to modulate the bunch length are shown.

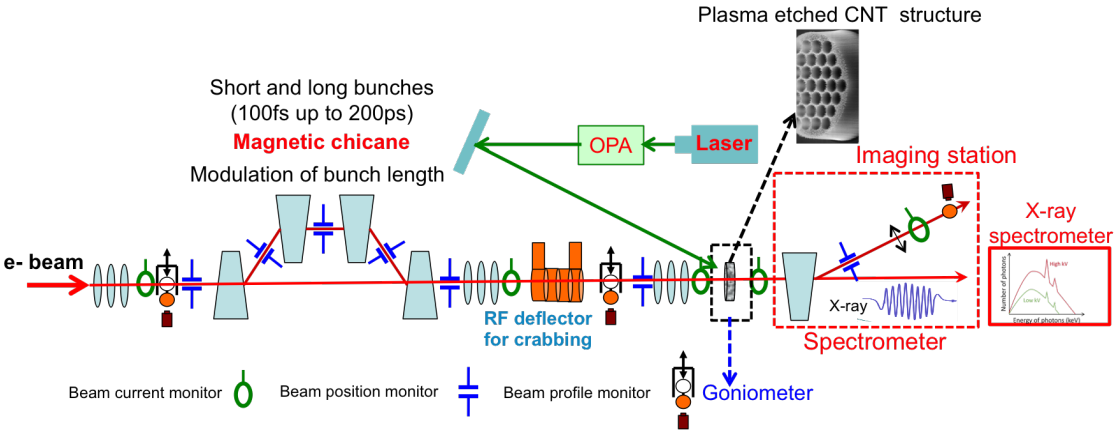

Figure 1. Proposed experimental layout with typical beam diagnostics equipment shown.

Beams will be focused into the experimental CNT sample by upstream quadrupole magnets. The CNT sample will be placed in a support/goniometer which will allow vertical and horizontal motion, as well as rotation in the horizontal plane. The sample can thus be centred with respect to the electron beam, and allows optimisation with respect to the incidence angle. Then, an initial laser pulse or electron beam driver may be used to excite plasmon and plasmon-polariton modes, which will be used to accelerate a suitably-timed trailing witness beam. Further, the CNT array will be irradiated by a tabletop femtosecond UV laser. Taking into account that metallic CNTs effectively behave as hollow plasma channels, if the photon-plasmon coupling condition is fulfilled, electromagnetic waves in the hollow channel can be excited. This will induce betatron oscillations in the electrons crossing the channels and will give rise to coherent radiation in X-ray regimes. This part of the experiment will also allow us to investigate the suitability of a photo-excited CNT array to be used as compact X-ray source.

3. Interaction with laser pulses

Particle-in-cell (PIC) simulations have been carried out using the PIConGPU code [14] with a temporally Gaussian, linearly polarised laser pulse. The laser parameters are: wavelength 55 nm, FWHM pulse length 5 fs and intensity $2.83 \times 10^{15}\,\mathrm{W/cm^2}$, corresponding to the normalised vector potential $a_0 = eA/m_e c = 2.5 \times 10^{-3}$. The intensity is restricted so as to avoid quick ionisation and ensure target survival. First, a 2D structure made of 10 layers of C^+ ions and electron pairs was generated with transverse dimensions shown in figure 2. This was extruded for 300 nm to be the size of a few laser wavelengths while remaining within the available computational resources. The mesh resolution was about 0.01 nm (10 mesh cells per layer thickness). Using the arrangement of the Carbon atoms in a typical graphene cell, the initial electrons density was set to $3.7 \times 10^{23}\,\mathrm{cm^{-3}}$. The corresponding plasma frequency and plasma wavelength are 5.46 PHz and 55 nm, respectively.

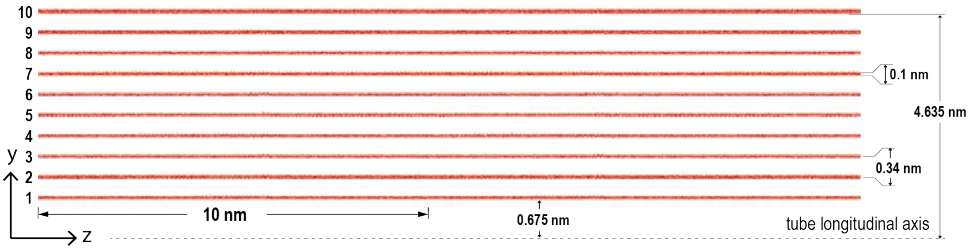

Figure 2. Transverse dimensions of the simulated structure: inner tube radius 0.675 nm, layer thickness 0.1 nm and gap between layers 0.34 nm. Numerically, the structure corresponds to 20 infinitely deep parallel plates. Only a side of the tube is shown.

Enabling tunnelling, barrier-suppression and collisional ionisation as implemented in PIConGPU, the effect of tuning the laser intensity was explored. Working with a simplified model, where the carbon ions move freely as in a gas, it was necessary to find an upper and lower bound to the laser intensity in order to both preserve target integrity and stimulate charge density modulation by ionisation. This effectively creates a separation from the virtually fixed carbon ions, driving electric fields along the tube. As shown in figure 3, the region between the cyan and green lines appears to be favourable. The results shown below are obtained for the cyan line.

Further increase of the laser intensity, such as that described by the orange curve, would lead to unrealistically large oscillations of the carbon ions. The simulation starts with a free electron for each C^+ ion. This electron stands for that in the delocalised π orbital, which accounts for electrical and thermal conduction in CNTs. In these simulations, all electrons and carbon ions are free to move longitudinally and transversely. The CNTs receive only a transverse electric field component E_y during the full pulse length of 15 fs. The electrons are set in periodic transverse (y) motion with elongations in the order of 0.1 nm, which co-propagate with the laser phase along the tube. In addition, due to ionisation there is electron gas between the layers, trapped in periodic motion around the carbon ions. The density of this inter-layer electrons gas bears the footprint of the fast passage of the laser pulse, and remains larger at places where the laser pulse acts at peak intensity; at every half-wavelength along the tube. A representation of the electric fields is shown in figure 4. The longitudinal (z) component of the electric field takes over its transverse (y) component at about $t = 18.025$ fs (98 laser periods). By this time, the inter-layer electrons gas is significantly bunched in transverse structures which advance as a density wave along the tube. However, there is a π phase lag between the two sides of the tube. Accordingly, the longitudinal (z) electric field is in anti-phase.

An enhancement of the longitudinal (z) electric field and electrons charge density plots is shown

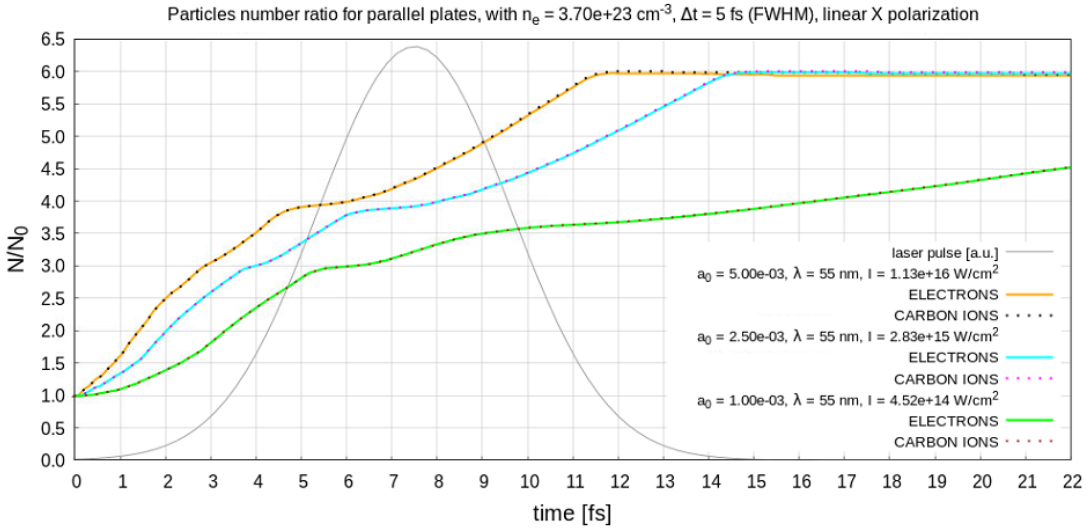

Figure 3. Various ionisation rates achieved within a very narrow range of a_0. The value $N/N_0 = 6$ indicates complete ionisation.

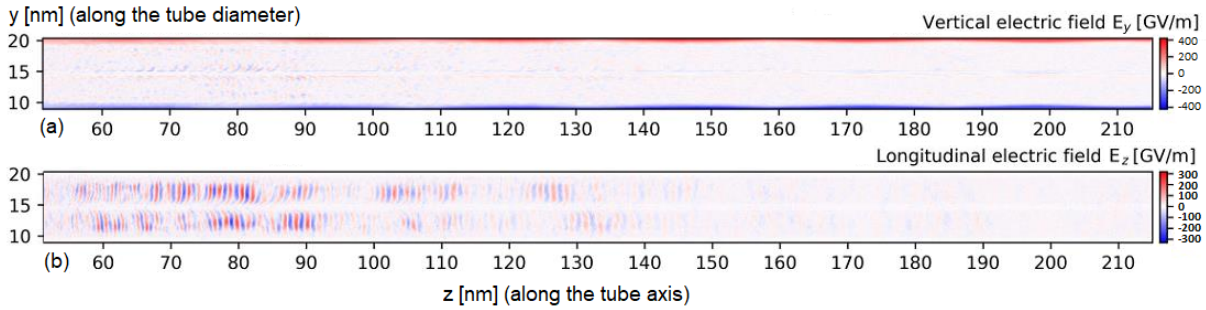

Figure 4. (top) transverse in-plane electric field, (bottom) longitudinal in-plane electric field in the layers region at $t = 18.025$ fs. The laser pulse moves to the right.

in figure 5. The plasmon resonates at a wavelength of about 1.5 nm and propages rightwards even after the laser pulse has passed.

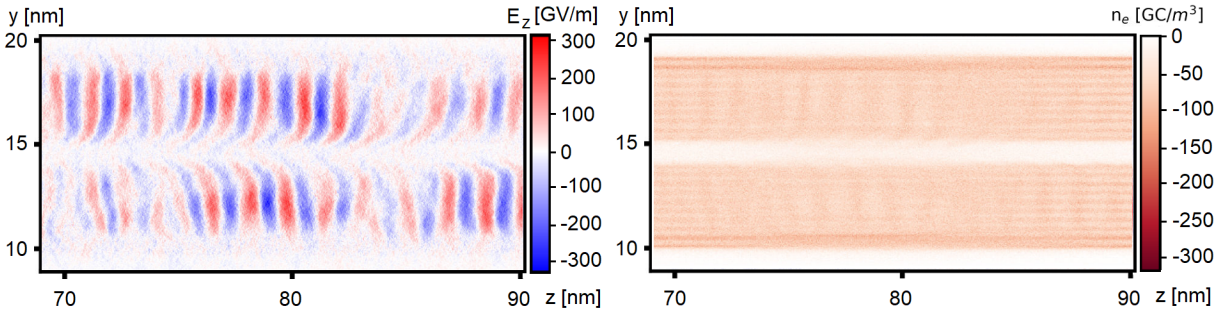

Figure 5. Zoom of the longitudinal in-plane electric field (left) and electrons charge density (right) at $t = 18.025$ fs. The laser pulse moves from left to right and its end is 1.1 µm away.

Although not shown here, the region around $z = 80$ nm is one in which the electron gas density

reaches a maximum, following the ionisation, long before (∼10 fs) the plasmon builds up. The passage of the plasmon through this region is strongly perturbed, as it can be seen around $z = 85$ nm, but established back, further to the right. Following the charge density wave, the plasmon field pattern moves from left to right in the trail of the laser pulse. Further numerical studies will explore conditions in which the longitudinal electric field can resonate long enough to be useful for acceleration behind the laser pulse. A few parameters such as the pulse length and the number of layers will be studied and the most favourable combinations will be used for more sophisticated 3D models.

4. Beam driven anisotropic model

Since their discovery [15] numerous works have modelled the electronic and electromagnetic properties of single- and multi-walled carbon nanotubes. The 2D thin-shell hydrodynamic model of hybrid electrostatic plasmon-phonon modes of [16, 17, 6] is of particular interest to charged particle acceleration. It has been adapted for electromagnetic surface plasmon polaritons (SSPs) propagating within (and leaking outside) the CNT by [18] for relativistic phase velocities, providing results consistent with experimentally measured properties. However, while these modes may be excited by propagating charged particle beams, such 2D thin-shell models are incapable of supporting the longitudinal oscillations ('volume' plasmon modes) driven directly by beam charge as presented in [19]. They also cannot provide the radial charge separation required to drive the highly nonlinear surface oscillations such as that proposed for a high-density plasma medium [5], or a general solid-state hollow channel accelerator [20] unless the CNT walls are pre-ionised, for example with a laser.

Here we present preliminary particle-in-cell simulations of thick CNT walls with orthotropically free electrons on a uniform positive (jellium) background. Analogously to graphene, such 'conduction band' electrons are immobile in the radial direction, r, but free to move in the axial, z, and azimuthal, ϕ directions. Modelled as a dielectric medium, this corresponds to a tensor dielectric function

$$\epsilon_a = \begin{pmatrix} \epsilon_r & 0 & 0 \\ 0 & \epsilon_\parallel & 0 \\ 0 & 0 & \epsilon_\parallel \end{pmatrix} \tag{1}$$

in (r, ϕ, z) coordinates, where $\epsilon_r = 1 - s\omega_p^2/\omega^2$ and $\epsilon_\parallel = 1 - \omega_p^2/\omega^2$, for conductivities in the ratio s between the r and z-ϕ directions ($s = 0$ for radially immobile electrons). Here, $\omega_p = \sqrt{n_0 e^2/\epsilon_0 m_e}$ is plasma frequency of quasi-free electrons of mass m_e, charge e, number density n_0, with vacuum permittivity ϵ_0.

4.1. Particle-in-cell code modifications

The particle push, as implemented [21] in the open-source 3D-Cartesian PIC code EPOCH [22], reads:

(i) advance position by half-step (first order), $\vec{r}_{n+1/2} = \vec{r}_n + \Delta t \vec{u}_n/(2\gamma_n)$;

(ii) advance momentum by half-step (first order), $\vec{u}_{n+1/2} = \vec{u}_n + e\vec{E}_{n+1/2}\Delta t/2$;

(iii) Boris push of momentum to $\vec{u}_{n+1}$ using $\vec{E}_{n+1/2}$ and $\vec{B}_{n+1/2}$;

(iv) advance position by half-step using $\vec{u}_{n+1}$, $\vec{r}_{n+1} = \vec{r}_{n+1/2} + \Delta t \vec{u}_{n+1}/(2\gamma_{n+1})$.

In the above, $\vec{r}_n$, $\vec{u}_n$, γ_n, $\vec{E}_n$, and $\vec{B}_n$, are the position, momentum and Lorentz factor of the particle, and the electric and magnetic field experienced by the particle at the n^{th} timestep, respectively. In order to simulate orthotropically free electrons, the above algorithm must be modified to ensure that particles do not leave their initial radius. However, when using a

finite time step, simply projecting the velocity onto the local to local ϕ-z plane causes the radial position to grow by $\Delta r^2 \approx \Delta t^2 u_\phi^2/\gamma^2 > 0$ at each step. Similarly, adding a first-order centripetal acceleration correction to $\vec{u}_{n+1}$ using $\vec{r}_{n+1/2}$ and $\vec{u}_{n+1}$ also leads to a radial increment $\Delta r^2 \gtrsim \Delta t^4 u_{\perp n+1}^4/\gamma^4 r_{n+1/2}^2$ even if $\vec{u}_{n+1}$ has no radial component. As the simulation progresses, this leads such particles to spuriously spiral outwards as they move azimuthally within the nanotube wall. Therefore, to avoid such outward motion, the push was modified so as to enforce constant radial position. Specifically, $\vec{E}_{n+1/2}$ is projected on to the local z-ϕ plane after step (i), and the magnetic torque used in step (iii) is projected on to the local r- direction after step (ii). Further, the transverse components of the position updates in (i) and (iv) are recast as rotations on the particle's cylinder. That is, a Cartesian drift to $(x_{m+},\ y_{m+})$ from $(x_m,\ y_m)$ over time δt of the form $\vec{r}_{m+} = \vec{r}_m + \vec{u}\Delta t/\gamma$, as found in (i) and (iv), is changed to the following update, giving the new position $(x^*_{m+},\ y^*_{m+})$, and a rotated momentum $(u_{x,m+},\ u_{y,m+})$:

$$\begin{pmatrix} x^*_{m+} & u_{x,m+} \\ y^*_{m+} & u_{y,m+} \end{pmatrix} = \begin{pmatrix} \cos\Delta\phi & -\sin\Delta\phi \\ \sin\Delta\phi & \cos\Delta\phi \end{pmatrix} \begin{pmatrix} x^*_m & u_{x,m} \\ y^*_m & u_{y,m} \end{pmatrix} \tag{2}$$

Here, $\Delta\phi = \frac{|\vec{u_n}|\Delta t}{2\gamma_n|\vec{r}_n|}$ for step (i), and $\Delta\phi = \frac{|\vec{u_n}+\vec{u}_{n+1}|\Delta t}{2\gamma_{n+1}|\vec{r}_n|}$ for step (iv). Note that due to the projection of the field quantities, $\vec{u}$ does not gain an r-component at any stage of the Boris push or overall process. The drift in step (iv) is done using the average of the initial and Boris-pushed momenta, which ensures a consistent, overall 2nd-order 'midpoint' scheme. Figure 6 shows preliminary 3D PIC simulation of implementation into a CNT driven by a (toy) beam in EPOCH with radius $\sigma_r = 10$ nm in a grid of $258 \times 258 \times 1690$ cells. The 20 nm thick

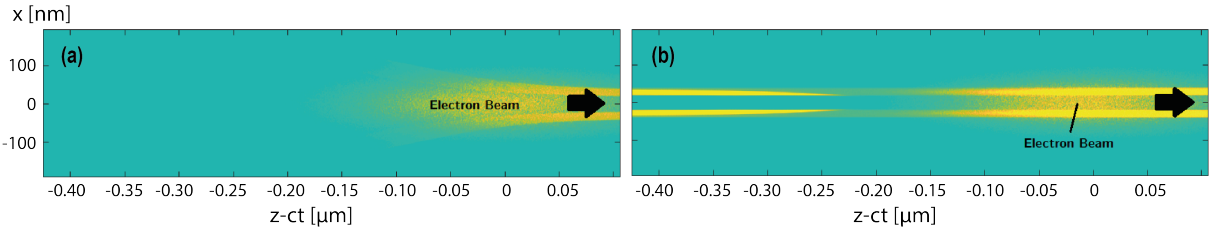

Figure 6. Comparison of electron density in EPOCH simulations of the interaction of a narrow electron bunch with a single CNT without (a) and with (b) radial confinement of electrons in the nanotube walls. Slice shown is across diameter of nanotube.

CNT wall around a 20 nm-radius hollow was modelled with pseudoparticles in a 1:1 ratio with physical electrons at a number density of 10^{25} m^{-3}, on a uniform *jellium* background with transverse resolution of 1 cell/nm. It is seen that opposed to previous simulations of non-linear perturbation in [19] where the CNT walls are strongly deformed, here a density perturbation is excited within the nanotube walls but remains confined.

5. Conclusions and Outlook

We presented 2D simulation results achieved for the interaction of UV laser pulses with a typical CNT structure. The appearance of an accelerating electric field resonating 1.5 nm with intensities in the order of a few hundreds of GV/m was demonstrated. This is notable due to the fact that the laser intensity was as low as 10^{15} W/cm^2. We have found also a peculiar damping phenomenon due to the larger-scale (10 nm) variation of the electron gas density along the tube. Preliminary implementation of radially bound particles into a particle-in-cell simulation is presented to model bound CNT-wall electrons. Further studies will improve the resonance of the fields behind the laser pulse and a multi-pulse operation mode could be found such that the

laser and electron bunch hit the target successively. Work on comprehensive testing of the PIC code modifications and implications on electromagnetic mode properties is ongoing. Finally, such models will be used to model and explore accelerating modes in a CNT array, which stands to inform the proposed proof-of-principle experiment.

Acknowledgments

The authors acknowledge support by STFC CDT LIV.DAT and by the STFC (UK) grant ST/P006752/1, as well as use of high-performance computing resources provided by STFC's SCARF cluster.

References

[1] Chen P 1986 A solid state accelerator *AIP Conf. Proc.* **156** 222
[2] Tajima T and Cavenago M 1987 Crystal Accelerator *Phys. Rev. Lett.* **59** 1440-3
[3] Shin Y M et al. 2017 Ultra-high gradient channeling acceleration in nanostructures: Design/progress of proof-of-concept (POC) experiments *AIP Conf. Proc.* **1812** 060009
[4] Zhang X et al. 2016 Particle-in-cell simulation of x-ray wakefield acceleration and betatron radiation in nanotubes *Phys. Rev. Accel. Beams* **19** 101004
[5] Shin Y M 2019 Carbon nanotube accelerator — Path toward TeV/m acceleration: Theory, experiment, and challenges *Int. J. Mod. Phys. A* **34** 1943005
[6] Moradi A 2013 *Photonic. Nanostruct.* Surface plasmon–polariton modes of metallic single-walled carbon nanotubes **11** 85-8
[7] Bhushan B 2017 *Springer Handbook of Nanotechnology* (Berlin: Springer) 215-6
[8] Batterman B W and Cole H 1964 Dynamical Diffraction of X Rays by Perfect Crystals *Rev. Mod. Phys.* **36** 681-717
[9] Murakami M and Tanaka M 2013 *Appl. Phys. Lett.* **102** 163101
[10] Clarke J et al. 2014 CLARA conceptual design report *J. Instrum.* **9**, T05001
[11] McIntosh P et al. 2016 The VELA and CLARA Test Facilities at Daresbury Laboratory, *Proc. of LINAC'16 (East Lansing, MI, USA)*
[12] Navarro Q et al. 2014 CALIFES: A Multi-Purpose Electron Beam for Accelerator Technology Tests *Proc. of LINAC'14 (Geneva)*
[13] Gamba D et al. 2018 The CLEAR user facility at CERN *Nucl. Instrum. Meth. Phys. Res. A* **909** 480
[14] Burau H et al. 2010 PIConGPU: A Fully Relativistic Particle-in-Cell Code for a GPU Cluster *IEEE T. Plasma. Sci.* **38**, 2831-2839
[15] Iijima S 1991 Helical microtubules of graphitic carbon *Nature* **354** 56–8
[16] Mowbray D J, Miškovic Z L, Goodman F O and Wang Y-N 2004 Interactions of fast ions with carbon nanotubes: Two-fluid model *Phys. Rev. B* **70** 195418
[17] Mowbray D J, Miškovic Z L and Goodman F O 2006 Ion interactions with carbon nanotubes in dielectric media *Phys. Rev. B* **74** 195435
[18] Wei L and Wang Y N 2004 Electromagnetic wave propagation in single-wall carbon nanotubes *Phys. Lett. A***333** 303-9
[19] Resta-López J et al. Study of Ultra-High Gradient Acceleration in Carbon Nanotube Arrays *Proc. IPAC 2018 (Vancouver, Canada)* (JACoW Publishing: Geneva, Switzerland)
[20] Sahai A A 2020 Solid-state tube wakefield accelerator using surface waves in crystals *Int. J. Mod. Phys. A* **34** 1943009
[21] Ruhl H Classical Particle Simulations with the PSC code *https://www.plasma-simulation-code.net/documentation/psc-docu.pdf*
[22] Arber T D et al. 2015 Contemporary particle-in-cell approach to laser-plasma modelling *Plasma Phys. Contr. F.* **57** 11